Molecular Therapy
Original Article

Radionuclide Imaging-Guided Chemo-Radioisotope Synergistic Therapy Using a ^{131}I-Labeled Polydopamine Multifunctional Nanocarrier

Zhiqiang Li,[1,2] Baikui Wang,[2] Zheng Zhang,[2] Bo Wang,[1] Qiangqiang Xu,[1] Wenjie Mao,[1] Jie Tian,[1,3] Kai Yang,[2] and Fu Wang[1]

[1]Engineering Research Center of Molecular and Neuro Imaging, Ministry of Education, School of Life Science and Technology, Xidian University, Xi'an, Shaanxi 710071, China; [2]State Key Laboratory of Radiation Medicine and Protection, School of Radiation Medicine and Protection and School for Radiological and Interdisciplinary Sciences (RAD-X), Collaborative Innovation Center of Radiation Medicine of Jiangsu Higher Education Institutions, Soochow University, Suzhou, Jiangsu 215123, China; [3]CAS Key Laboratory of Molecular Imaging, Institute of Automation, Chinese Academy of Sciences, Beijing 100190, China

Development of biocompatible nanomaterials with multiple functionalities for combination of radiotherapy and chemotherapy has attracted tremendous attention in cancer treatment. Herein, poly(ethylene glycol) (PEG) modified polydopamine (PDA) nanoparticles were successfully developed as a favorable biocompatible nanoplatform for co-loading antitumor drugs and radionuclides to achieve imaging-guided combined radio-chemotherapy. It is demonstrated that PEGylated PDA nanoparticles can effectively load two different drugs including sanguinarine (SAN) and metformin (MET), as well as radionuclides ^{131}I in one system. The loaded SAN and MET could inhibit tumor growth via inducing cell apoptosis and relieving tumor hypoxia, while labeling PDA-PEG with ^{131}I enables *in vivo* radionuclide imaging and radioisotope therapy. As revealed by the therapeutic efficacy both in cell and animal levels, the multifunctional PDA nanoparticles (^{131}I-PDA-PEG-SAN-MET) can effectively repress the growth of cancer cells in a synergistic manner without significant toxic side effects, exhibiting superior treatment outcome than the respective monotherapy. Therefore, this study provides a promising polymer-based platform to realize imaging-guided radioisotope/chemotherapy combination cancer treatment in future clinical application.

INTRODUCTION

Cancer has been one of the most fatal diseases affecting human healthcare for many years.[1] So far, chemotherapy, radiotherapy, and surgery are still the major clinical approaches for cancer treatment.[2–5] However, single therapy including radiotherapy and chemotherapy always suffers from some side effects, such as multidrug resistance, inefficient uptake, or nonspecific distribution of drugs, making it difficult to achieve favorable therapeutic outcomes.[6–8] In the past few years, multi-functional nanoparticles have been widely used in the fundamental research and clinical practices to improve the bioavailability, pharmacokinetics, and tumor targeting of therapeutic drugs.[9–13] Hence, the development of multifunctional nanocarriers as platform to realize combined radiotherapy and chemotherapy would have great potential for cancer treatment.

Among the various nanomaterials that are employed in nanomedicine field, polydopamine (PDA) has received tremendous attention due to its great surface modification ability and biocompatibility. In addition, another outstanding feature of PDA is that its chemical structure makes it easier to incorporate many functional groups such as amine, catechol, and imine.[14–17] These functional groups could be utilized as anchors for loading of anticancer drugs and covalently modifying with desired radionuclides simultaneously, which would provide significant potential to realize the combined chemotherapy and radioisotope therapy in one nanoparticle system by virtue of its powerful biocompatible capability.[18–21]

In this study, we developed a PDA-based multifunctional nanocarrier by loading with two types of anticancer drug and a radionuclide to achieve imaging-guided chemo-radioisotope synergistic therapy in the cancer treatment (Figure 1). To improve the biocompatibility, the self-polymerized PDA nanoparticles were modified with polyethylene glycol (PEG) in this nanocarrier. Radionuclide ^{131}I, which emits strong gamma and beta rays, was conjugated on PDA-PEG nanoparticles and serves as gamma imaging and a radiotherapy agent. Meanwhile, two different anticancer drugs, sanguinarine (SAN) and metformin (MET), were also loaded on PDA nanoparticles for cancer chemotherapy. SAN is a benzophenanthridine alkaloid that could

Received 1 January 2018; accepted 20 February 2018;
https://doi.org/10.1016/j.ymthe.2018.02.019.

Correspondence: Kai Yang, State Key Laboratory of Radiation Medicine and Protection, School of Radiation Medicine and Protection and School for Radiological and Interdisciplinary Sciences (RAD-X), Collaborative Innovation Center of Radiation Medicine of Jiangsu Higher Education Institutions, Soochow University, Suzhou, Jiangsu 215123, China.
E-mail: kyang@suda.edu.cn
Correspondence: Fu Wang, Engineering Research Center of Molecular and Neuro Imaging, Ministry of Education, School of Life Science and Technology, Xidian University, Xi'an, Shaanxi 710071, China.
E-mail: fwang@xidian.edu.cn

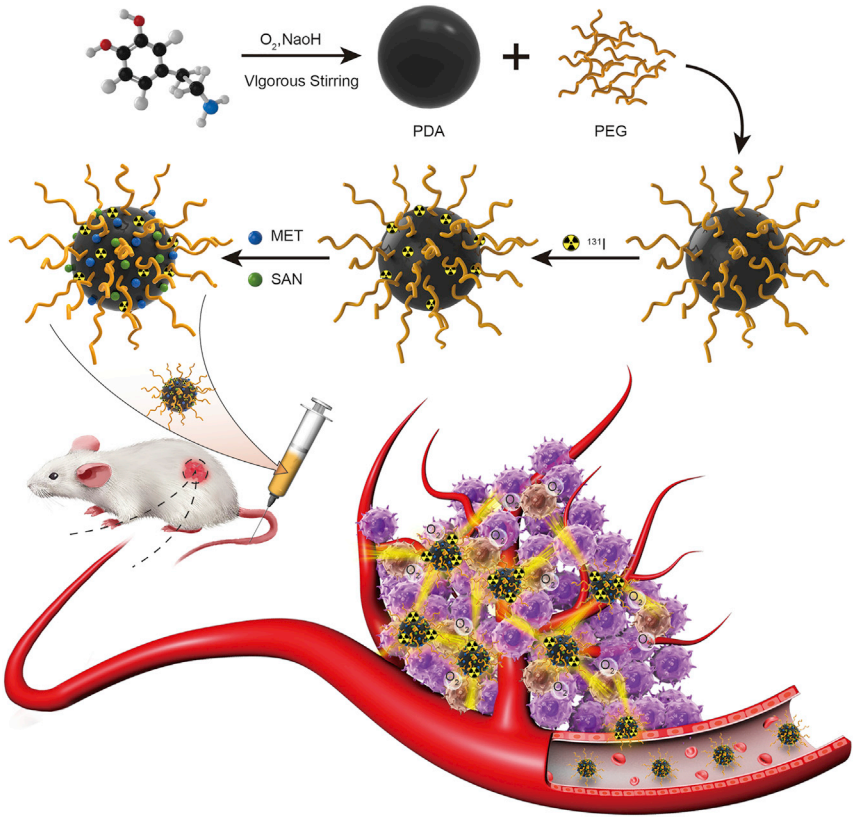

Figure 1. Schematic Illustration of the PDA-Based Nanoparticles for Combined Chemo-Radiotherapy
Dopamine hydrochloride was polymerized under vigorous stirring and functionalized with PEG. The PDA-PEG was then labeled with radionuclide ^{131}I, as well as small molecular drugs SAN and MET. The obtained ^{131}I-PDA-PEG-SAN-MET nanoparticles could be used as multi-functional therapeutic agents for radionuclide imaging guided combination therapy.

induce apoptosis via activating the production of reactive oxygen species (ROS) in cancer cells,[22] while MET is a potent inhibitor of respiration that could increase the oxygen content in tumor microenvironment and thus dramatically improve radiotherapy efficacy.[23] Radionuclide imaging showed efficient tumor uptake in xenografts injected with ^{131}I-PDA-PEG nanoparticles. Compared with the respective monotherapy groups, the combined chemo-radioisotope therapy group treated by ^{131}I-PDA-PEG-SAN-MET nanoparticles exhibited an obviously synergistic therapeutic efficacy in mouse tumor model with no significant toxicity. Therefore, our study demonstrated that PEGylated PDA nanoparticle could serve as a promising nanoplatform to realize imaging-guided synergistic therapy in cancer treatment by incorporating with various imaging and therapeutic agents.

RESULTS AND DISCUSSION

Synthesis and Characterization of PDA Nanoparticles

In this work, PDA nanoparticles was synthesized from dopamine hydrochloride via a straightforward approach according to our previous protocol.[18] In brief, dopamine hydrochloride was polymerized by vigorous stirring in the presence of sodium hydroxide (1 M) at pH 10.0. After 5 hr of reaction, the color of solution changed from yellow to dark brown, indicating that PDA nanoparticles were formed. As determined by transmission electron microscopy (TEM) (Figure 2A) and dynamic light scattering (DLS) (Figure 2B), the yielded PDA nanoparticles showed uniform spherical morphology with an average hydrodynamic size of ~110 nm. To improve the water solubility of PDA, amine-terminated PEG (100 kD) was used to functionalize PDA nanoparticles under pH 10.0 to obtain PDA-PEG nanoparticles, which demonstrated enhanced stability in different physiological solutions including PBS, cell medium and fetal bovine serum (FBS) (Figure 2C). The average hydrodynamic size of PDA-PEG became larger (~200 nm) due to PEG coating (Figure 2B). Moreover, both PDA and PDA-PEG solution showed broad absorption from UV to near-infrared (NIR) band ranges as recorded by UV-vis-NIR spectrum (Figure 2D).

Drug Loading and Radiolabeling of PDA-PEG

Given the great surface modification ability of PDA, we then test whether PDA could load various anticancer drugs and radionuclides. SAN, a natural product with broad spectrum of anticancer activity, and MET, a potent inhibitor of respiration, were found to be successfully co-loaded on the surface of PDA-PEG via hydrophobic/electrostatic interaction. As measured by UV-vis-NIR spectrum, an absorbance peak of 330 nm was superimposed on the absorption spectrum of the obtained PDA-PEG-SAN-MET nanoparticles, further indicating that SAN and MET drugs were successfully loaded onto PDA-PEG nanoparticles (Figure 2D). However, compared with PDA-PEG, the hydrodynamic size of PDA-PEG-SAN-MET didn't change too much after loading of drugs (Figure 2B). The SAN or MET loading ratio (SAN: PDA, MET: PDA, w/w) increased with increasing amounts of added SAN or MET (Figures 3A and 3B). UV-vis-NIR spectrum was also utilized to record the respective SAN or MET loading, further confirming that SAN and MET were loaded successfully onto the surface of PDA-PEG (Figures S1A and S1B). Considering the fact that too much SAN or MET loading would affect the stability of nanoparticles, the PDA-PEG: SAN: MET weight ratio of 1:1:2 was prepared to achieve an appropriate loading efficiency and was used for our followed experiments. The drug release behavior of PDA-PEG-SAN-MET nanoparticles was determined at different pH (5.3 or 7.4) and accelerated drug release was found at low pH due to the positive charge of SAN or MET (Figures 3C and 3D). Since ^{131}I can emit strong both β and γ rays,[24] ^{131}I is not only particularly used for

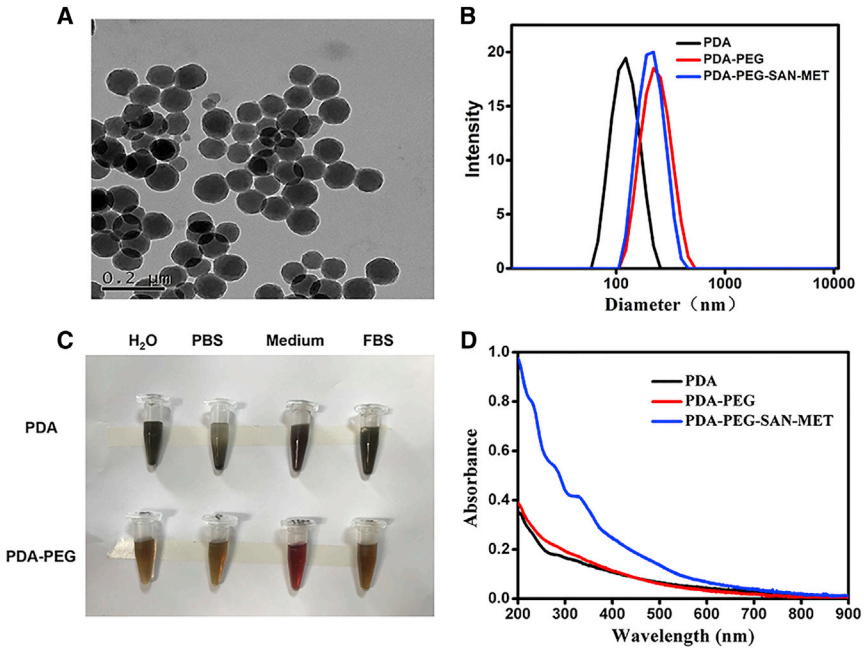

Figure 2. Preparation and Characterization of PDA Nanoparticles

(A) Transmission electron microscopy (TEM) images of PDA nanoparticles. (B) Size distribution of PDA, PDA-PEG, and PDA-PEG-SAN-MET in water measured by dynamic light scattering (DLS). (C) The stability of PDA and PDA-PEG in H_2O, PBS, 1640 medium and fetal bovine serum (FBS). (D) UV-vis–NIR spectra of PDA, PDA-PEG, and PDA-PEG-SAN-MET.

radiotherapy, but also used as a contrast agent for gamma imaging. To achieve imaging-guided internal radiotherapy, ^{131}I was utilized to label PDA-PEG via electrophilic substitution reaction in the presence of iodogen. It was found that the obtained ^{131}I-PDA-PEG showed a high radiolabeling efficiency at 80%, as well as good radiolabeling stability in PBS and serum after 24 incubation at 37°C (Figure 3E).

In Vitro Cytotoxicity and Apoptosis Induced by PDA Nanoparticles

Before studying the *in vivo* therapeutic efficacy of ^{131}I-PDA-PEG-SAN-MET, we first investigated the intracellular delivery behavior of the nanoparticles. The 4T1 murine breast cancer cells were incubated with Cy5.5-labeled PDA-PEG-SAN-MET and then imaged by a confocal fluorescence microscope after 6 hr of incubation. It was found that strong red fluorescence signal came from the cytoplasm of cells, indicating that these nanoparticles were efficiently uptaken by cells (Figure 4A). We then examined the potential cytotoxicity of nanoparticles using the cell counting kit-8 (CCK-8) assay. 4T1 cells were incubated with PDA-PEG, free ^{131}I, free SAN, ^{131}I-PDA-PEG, PDA-PEG-SAN, PDA-PEG-SAN-MET and ^{131}I-PDA-PEG-SAN-MET at different concentrations for 24 hr. As shown in Figure 4B, PDA-PEG had no obvious toxicity to 4T1 cells even at a high concentration of 500 μg/mL, suggesting that PDA-PEG nanoparticles have a great biocompatibility. We then investigated the toxicity of the free SAN, PDA-PEG-SAN and PDA-PEG-SAN-MET, and found that there was no obvious difference with the cell viability after loading with SAN or MET on PDA-PEG at the same concentration of SAN (Figure 4C). We next examined the potential cytotoxicity of ^{131}I-PDA-PEG and free ^{131}I. The results demonstrated that ^{131}I-PDA-PEG was more toxic than free ^{131}I at the high dose of ^{131}I (Figure 4D), which might be attributed to the increased cellular uptake of ^{131}I via PDA-PEG. To perform the combined radio-chemotherapy, 4T1 cells were incubated with ^{131}I-PDA-PEG, PDA-PEG-SAN-MET and ^{131}I-PDA-PEG-SAN-MET at various concentrations for 24 hr. ^{131}I-PDA-PEG-SAN-MET exhibited the most superior cytotoxicity at the high concentration compared with the single treatment with ^{131}I-PDA-PEG or PDA-PEG-SAN-MET (Figure 4E), indicating that combined radio-chemotherapy based on ^{131}I-PDA-PEG-SAN-MET nanoparticles achieved a synergistic effect in killing cancer cells.

To explore the underlying mechanism by which nanoparticles repressed cell viability, we examined whether the inhibitory effect on cell viability was resulted from cell apoptosis. The 4T1 cells were treated with different amounts of PDA-PEG-SAN. Then flow cytometry was performed and the results demonstrated that the percentage of Annexin V-positive cells increased along with the increased concentration of PDA-PEG-SAN (Figures 5A and 5B). Furthermore, we used Ac-DEVD-pNA, a commercial caspase-3 substrate probe, to measured cellular caspase-3 activity from the cytosolic extracts of 4T1 cells after treatment with different dose of PDA-PEG-SAN. As shown in Figure 5C, the absorbance at 450 nm increased with the dose of nanoparticles, indicating the activated caspase-3 activity induced by PDA-PEG-SAN. In summary, these data suggest that PDA-PEG-SAN triggered apoptosis and thus affect cell viability in 4T1 cancer cells.

In Vivo Behavior of Radioisotope-Labeled PDA-PEG Nanoparticles

Since ^{131}I could act as a contrast agent for gamma imaging, we then employed gamma imaging to track the *in vivo* behaviors of ^{131}I labeled nanoparticles in the 4T1 tumor-bearing mice. The thyroids of mice were pre-blocked with cold NaI and then were intravenously (i.v.) injected with free ^{131}I (200 μCi of ^{131}I) or ^{131}I-PDA-PEG (10 mg/kg of PDA-PEG, 200 μCi of ^{131}I). As shown in Figure 6A, free ^{131}I were quickly eliminated from mice body without showing any obvious accumulation in tumors 24 hr post-injection. In contrast, the mice treated with ^{131}I-PDA-PEG exhibited conspicuous tumor

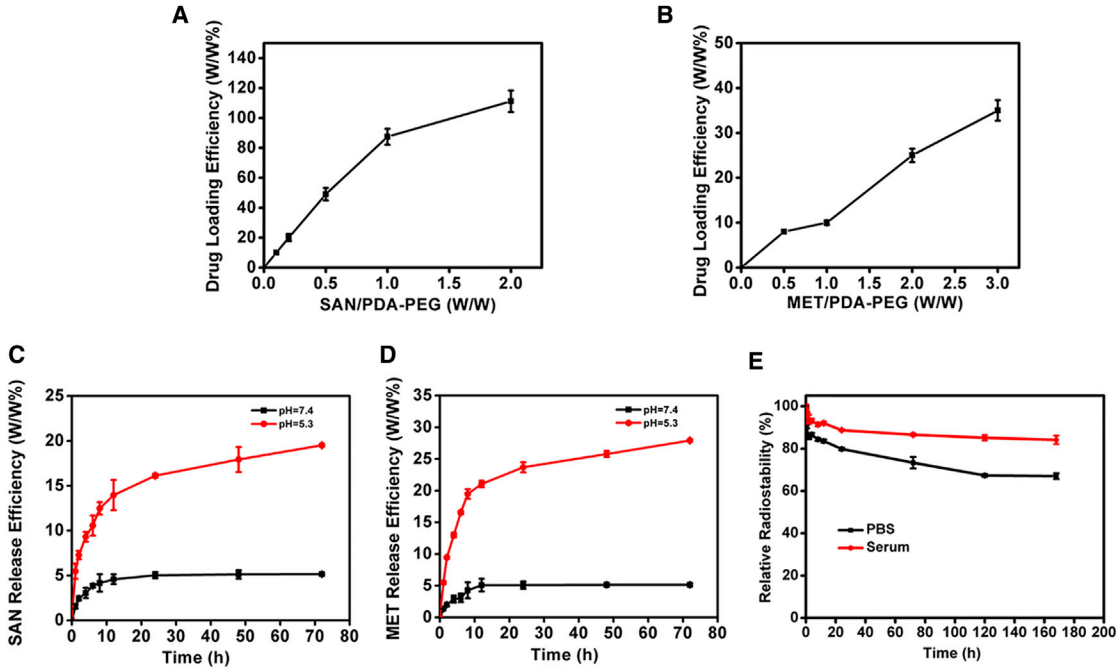

Figure 3. Drug Loading and Radiolabeling on PDA-PEG

(A and B) Quantification of SAN (A) or MET (B) loading at different feeding amounts of SAN or MET. (C and D) Release of SAN (C) or MET (D) from PDA-PEG nanoparticles at pH 5.3 or pH 7.4, respectively. (E) The radiostability of ^{131}I-PDA-PEG after incubation in PBS or serum.

accumulation for as long as 72 hr, likely due to the enhanced permeability and retention (EPR) effect.

To further study the *in vivo* behaviors of nanoparticles, we then investigated the blood circulation and biodistribution of ^{131}I-PDA-PEG-SAN-MET. The 4T1 tumor-bearing mice were i.v. injected with ^{131}I-PDA-PEG-SAN-MET (200 μCi of ^{131}I, 10mg/kg of PDA-PEG) and the blood was harvested from mice at different time points. Then the blood samples were measured to determine the radioactivity using a gamma counter. As shown in Figure 6B, the blood circulation half-lives of ^{131}I-PDA-PEG-SAN-MET exhibited a prolonged time ($t_{1/2}$ = 2.11 hr, $t'_{1/2}$ = 20.31 hr), abiding by a two-compartment model. For the biodistribution experiment, the major organs and tumors were collected for radioactivity measurement at 24 hr post-injection. Substantial uptake of ^{131}I-PDA-PEG-SAN-MET was observed in tumor, as well as in reticuloendothelial systems (RESs) including liver and spleen (Figure 6C).

In Vivo Combined Radio-Chemotherapy Based on PDA-PEG Nanoparticles

Encouraged by the superior therapeutic efficiency of PDA-based single chemotherapy or radiotherapy to cancer cells, we then employed ^{131}I-PDA-PEG-SAN-MET as a multifunctional agent for combined internal radiotherapy and chemotherapy in the mice model. The nude mice bearing 4T1 tumors were randomly divided into seven groups with five mice per group. These groups were treated with the following: (1) control; (2) PDA-PEG (10 mg/kg); (3) PDA-PEG-SAN (4 mg/kg of SAN); (4) PDA-PEG-SAN-MET (4 mg/kg of SAN); (5) ^{131}I-PDA-PEG (200 μCi of ^{131}I); (6) ^{131}I-PDA-PEG-SAN (4 mg/kg of SAN, 200 μCi of ^{131}I); and (7) ^{131}I-PDA-PEG-SAN-MET (4 mg/kg of SAN, 8 mg/kg of MET, 200 μCi of ^{131}I). The aforementioned nanoparticles were i.v. injected in mice every 3 days for four times. As shown in Figure 7A, compared to PBS or free PDA-PEG treated group, chemotherapy (PDA-PEG-SAN or PDA-PEG-SAN-MET) or radiotherapy (^{131}I-PDA-PEG) alone group could only slightly reduce tumor growth. In contrast, the combination therapy with ^{131}I-PDA-PEG-SAN-MET or ^{131}I-PDA-PEG-SAN was found to greatly inhibit tumor growth of mice, indicating the significant synergistic effect during combination therapy. Meanwhile, the mouse body weight has no obvious change with different treatments during the entire process (Figure 7B). Notably, ^{131}I-PDA-PEG-SAN-MET treatment group showed more effective than ^{131}I-PDA-PEG-SAN, likely owing to the fact that MET could relieve tumor hypoxia via reducing tumor oxygen consumption and thus result in improved therapeutic outcomes under the radiotherapy. To confirm this speculation, we used Pimonidazole, a hypoxia-specific probe that binds with thiol-containing proteins in hypoxic cells, to trace the tumor hypoxia state. Meanwhile, anti-mouse CD31 antibody was used to locate blood vessels inside the tumor. As revealed by the immunofluorescence imaging (Figure 7C), the tumors treated with ^{131}I-PDA-PEG-SAN-MET exhibited obviously relieved tumor hypoxia comparing with the control group. Therefore, the excellent effect achieved in the ^{131}I-PDA-PEG-SAN-MET treatment is due to the improved tumor oxygenation after the taking MET

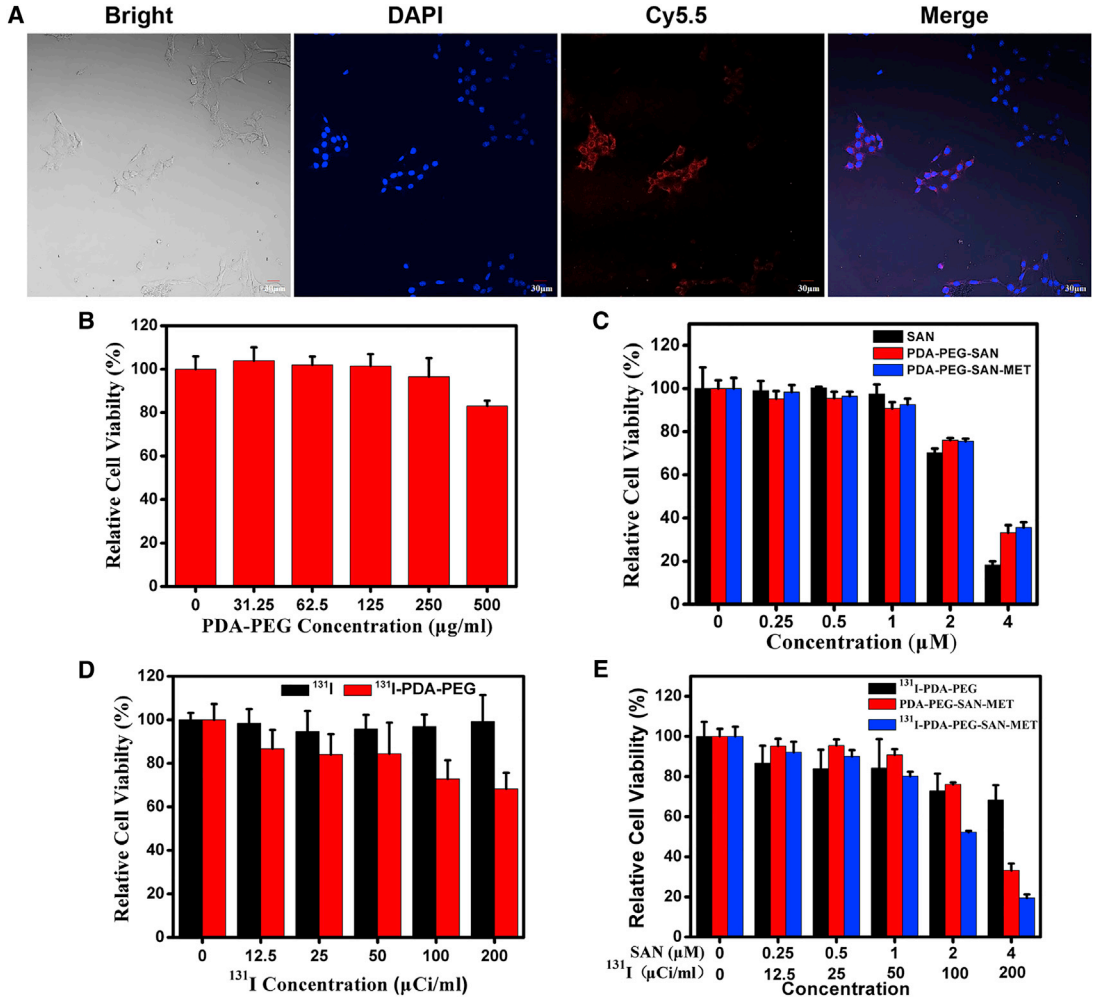

Figure 4. The Cellular Uptake, *In Vitro* Chemotherapy, and Radioisotope Therapy Efficacy of Nanoparticles

(A) Confocal fluorescence imaging of 4T1 cells that were incubated with Cy5.5-labeled PDA-PEG-SAN-MET for 6 hr. (B) The relative cellular viabilities of 4T1 cells after incubation with different concentrations of PDA-PEG for 24 hr. (C) The relative cellular viabilities of 4T1 cells after incubation with different concentrations of free SAN, PDA-PEG-SAN and PDA-PEG-SAN-MET for 24 hr. (D) The relative cellular viabilities of 4T1 cells after being incubated with different concentrations of free ^{131}I and ^{131}I-PDA-PEG (0.10, 0.20, 0.41, 0.83, and 1.65 μg/mL PDA-PEG) for 24 hr. (E) The relative cellular viabilities of 4T1 cells after being incubated with different concentrations of ^{131}I-PDA-PEG, PDA-PEG-SAN-MET and ^{131}I-PDA-PEG-SAN-MET (0.10, 0.20, 0.41, 0.83, and 1.65 μg/ml PDA-PEG) for 24 hr. All data are shown as mean ± SD of three independent experiments.

into caner by PDA-PEG nanoparticles. Taken together, it is obvious that combining chemotherapy with radiotherapy using PEGylated PDA nanoparticles as the nanocarrier offers remarkable advantages in cancer treatment with greatly enhanced therapeutic efficacy.

Conclusions

In summary, a biocompatible nanomaterial based on PDA combining chemotherapy and radiotherapy was constructed by simply mixing ^{131}I-labeled PDA with SAN and MET. In this study, we synthesized PDA nanoparticles through spontaneous air oxidation of dopamine under basic pH condition. PDA nanoparticles around 110 nm showed excellent dispersion stability in biological media and good biocompatibility in 4T1 cells after the appropriate surface modification with amine-terminated PEG. PEGylated PDA could be conveniently labeled with radionuclide ^{131}I with high radiolabeling yields and stabilities in mouse plasma. In the meantime, PDA-PEG nanoparticles were found to be loaded with SAN and MET with high drug loading efficiency. While ^{131}I labeling enables radionuclide imaging to real-time track the distribution of nanoparticles *in vivo* and make inner irradiation to the tumor, conjugation of ^{131}I and loading of SAN/MET make the obtained ^{131}I-PDA-PEG-SAN-MET nanoparticles an excellent nano-agent for combined radio-chemotherapy, which offers great synergistic therapeutic outcomes as is expected *in vivo* combined treatment. Moreover, MET delivered into the tumors by PDA-PEG nanoparticles could obviously enhance the tumor local oxygen level, overcome hypoxia-associated radioresistance and thus

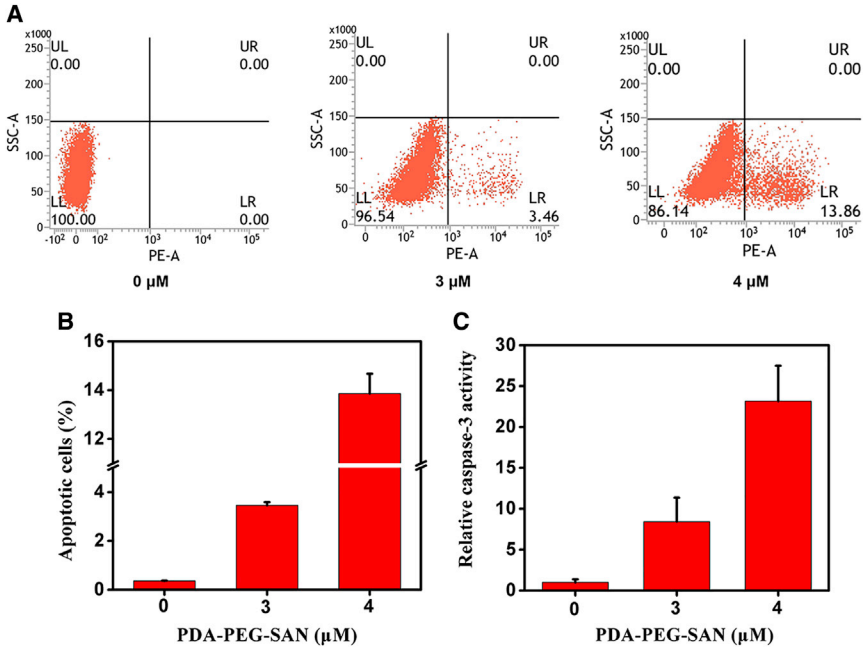

Figure 5. Cell Apoptosis Induced by PDA-PEG-SAN Nanoparticles

The 4T1 cells were treated with different concentrations (0, 3, 4 μM of SAN and 0, 1.24, 1.65 μg/mL PDA-PEG) of PDA-PEG-SAN nanoparticles for 24 hr. (A) The cells stained with FITC-Annexin V/PI kit were collected for flow cytometry analysis. (B) The quantification of the flow cytometry from three independent experiments. The apoptotic cells were determined by the percentage of Annexin V (+)/PI (−) cells. (C) Caspase-3 activity from the cells that were treated the same as (A). The cells were incubated with Ac-DEVD-pNA, a substrate for caspase-3. Then the released fluorescence products were measured using a caspase-3 activity assay kit. All data are shown as mean ± SD of three independent experiments.

improve radiotherapy efficacy. Therefore, our work presents a PDA-based nano-platform for imaging-guided *in vivo* synergistic chemo-radiotherapy and offers significant potential for clinical application in cancer combination treatment.

MATERIALS AND METHODS

Synthesis and Functionalization of PDA Nanoparticles

PDA nanoparticles were synthesized by a straightforward approach according to our published protocols with a little modification.[18] Simply, 180 mg of dopamine hydrochloride (Aldrich Chemical) was dissolved in 90 mL of double distilled water, then 760 μL of sodium hydroxide (NaOH, 1 mol/L) was added into the solution at 50°C under magnetic staining. After 5 hr of polymerization, black granular nanoparticles were collected by centrifugation at 14,000 rpm and washed with double distilled water for several times. The as-made PDA nanoparticles was covalently functionalized with amine-terminated PEG (mPEG-NH_2, 5 kDa). Five milliliters (1 mg/mL) of PDA nanoparticle was mixed with 50 mg of PEG-NH_2, which was dissolved in 2 mL double distilled water at pH 10.0 with magnetic stirring for 30 min. The mixture was stirred over 8 hr at room temperature, and then purified by filtration to remove excess PEG through 10 kDa molecular weight cut-off (MWCO) Amicon filters. The yielded nanoparticles were stored under 4°C for future experiments.

Drug Loading and Release

Small molecular drug SAN and MET were co-loaded on the surface of PDA-PEG nanoparticles via π-π stacking. In brief, 1 mL of PDA-PEG solution (0.5 mg/mL) was mixed with different amounts of SAN or MET (0.1–2 mg) in 2 mL of double distilled water at pH 7.3. The solution was stirred for 6 hr. Excess unloading SAN or MET was removed by centrifugation through 10 kDa MWCO filters. The final nanoparticles were re-suspended in double distilled water and stored at 4°C for further experiments. The drug loading efficiency was measured by UV-vis NIR. For drug release experiment, PDA-PEG-SAN or PDA-PEG-MET solutions were dissolved in double distilled water at different pH (5.3–7.3) in the 37°C water bath. At different time points, SAN or MET released from nanoparticles was collected and measured by UV-vis-NIR spectra. The final nanoparticles (PDA-PEG-SAN-MET) for combination therapy was made by PDA-PEG: SAN: MET at the mass ratio 1:1:2 using the above-mentioned method.

^{131}I Labeling, Radiolabeling Stability, and Radionuclide Imaging

PDA-PEG was labeled with radionuclide ^{131}I (Shanghai GMS pharmaceutical) by an Iodogen iodide method. Briefly, 150 μCi of ^{131}I and 1 mL of PDA-PEG nanoparticles (0.5 mg/mL) were simultaneously added into an Eppendorf (EP) tube, which was pre-coated with Iodogen (0.5 mg/mL). The mixture was reacted for 20 min at 25°C. Excess ^{131}I was removed by centrifugation through Amicon filters (MWCO = 10 kDa) and washed until no detachable radioactivity.

For the radiolabeling stability experiment, 1 mL of the obtained ^{131}I-PDA-PEG (1 mg/mL) was dissolved in 50 mL of PBS or serum in 37°C water bath. Free ^{131}I was scoured off by centrifuge through Amicon filters (MWCO = 10 kDa) and washed with double distilled water three times. The nanoparticles were collected for measuring the amount of retained ^{131}I by gamma counting. Finally, the ^{131}I-PDA-PEG nanoparticles was used to co-load SAN and MET at the mass ratio 1:1:2 (^{131}I-PDA-PEG: SAN: MET) for 6 hr.

For the radionuclide imaging, the free ^{131}I (200 μCi of ^{131}I) or ^{131}I-PDA-PEG (10 mg/kg of PDA-PEG, 200 μCi of ^{131}I) were i.v. injected into 4T1 tumors bearing mice with thyroid blocked with pre-injection of cold NaI and imaged by *in vivo* animal nuclide imaging system (Kodak, FX Pro) at various time points post injection.

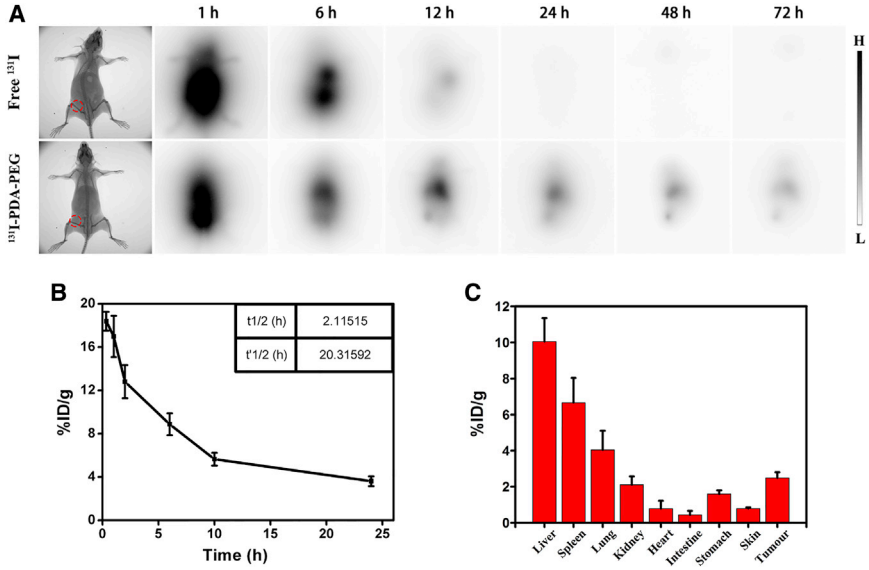

Figure 6. *In Vivo* Imaging and Biodistribution of ^{131}I Labeled PDA-PEG

(A) Gamma imaging of mice bearing 4T1 tumors after i.v. injection of free ^{131}I (200 μCi) or ^{131}I-PDA-PEG (10 mg/kg of PDA-PEG, 200 μCi of ^{131}I) at different time point. (B) The blood circulation curve of ^{131}I-PDA-PEG-SAN-MET nanoparticles (200 μCi of ^{131}I, 10 mg/kg of PDA-PEG) that were i.v. injected into tumor bearing mice. (C) The biodistribution of the same dose of ^{131}I-PDA-PEG-SAN-MET measured at 24 hr post injection into tumor bearing mice.

Cell Viability Assay

4T1 cells were cultured in RPMI-1640 medium supplemented with 1% penicillin-streptomycin and 10% FBS at 37°C in a 5% CO_2 containing humidified atmosphere. The *in vitro* cytotoxicity was measured by CCK-8 assay. The 4T1 cells were seeded into a 96-well plate at a density of 8,000 cells per well overnight and then incubated with different concentrations of PDA-PEG, free ^{131}I, free SAN, ^{131}I-PDA-PEG, PDA-PEG-SAN, PDA-PEG-SAN-MET, or ^{131}I-PDA-PEG-SAN-MET, respectively, for further 24 hr. CCK-8 assay was performed to determine the relative cell viabilities.

Cy5.5 Labeling and Cellular Uptake Assay

Two microliters of NHS-Cy5.5 (10 mg/mL) was mixed with 1 mL of PDA-PEG solution (2 mg/mL) and stirred overnight in the dark-field at room temperature. Free Cy5.5 was removed by centrifugation through Amicon filters (MWCO = 10 kDa) and washed three times with double distilled water until no detachable color in the filtration solution. For the cellular uptake, Cy5.5 labeled PDA-PEG nanoparticles were added into prepared 24 well plate (4×10^4 cells per well) for 6 hr. Then cells were washed by PBS and stained with 4′, 6-diamidino-2-phenylindole (DAPI) and then imaged by confocal microscope (Lecia SP5II laser scanning confocal microscope).

Flow Cytometry Analysis

The apoptosis of 4T1 cells induced by PDA-PEG-SAN was detected using an Annexin V-FITC/PI Apoptosis Detection Kit (BD PharMingen, MI) described previously.[25] Briefly, 4T1 cells pre-seeded into six cell plates were incubated with different concentrations of PDA-PEG-SAN (0 μM, 3 μM, 4 μM) for 24 hr. Then the cells were washed by PBS and collected in 2 mL EP tubes (5×10^4 cells per tube). The 4T1 cells were centrifuged at 1,000 rpm for 5 min to remove supernatant. Then the pellets were resuspended in binding buffer and Annexin V-FITC for 15 min at room temperature. Finally PI (5 μg/mL) was added and the apoptotic cells were analyzed using a flow cytometer (C6, BD PharMingen, MI, USA).

In Vitro Caspase-3 Activity Assay

The caspase-3 activity was measured using a caspase-3 activity assay kit (Beyotime Biotechnology, China) according to our previous method.[22] Briefly, the 4T1 cells were treated with different concentrations of PDA-PEG-SAN (0 μM, 3 μM, 4 μM) for 24 hr. The cells were then harvested and lysed in lysis buffer for 15 min. Afterward, the supernatants were collected by centrifuging at 14,000 rpm for 10 min. The Ac-DEVD-pNA (2 mM) was added to each sample and incubated for 2 hr at 37°C. The optical density of each sample was finally measured at a wavelength of 405 nm using a spectrophotometer (Shimadzu, Japan). The p-NA standard was used to calibrate the caspase-3 activity of each sample.

Blood Circulation and Biodistribution

For the blood circulation analysis, the healthy female Balb/C mice were i.v. injected with ^{131}I-PDA-PEG-SAN-MET nanoparticles (200 μCi of ^{131}I, 10 mg/kg of PDA-PEG per mouse). At each time point, about 15 μL of blood were drawn from one side of orbital venous plexus of mouse. The radioactivity in each blood sample was then measured by a gamma counter (LB211, Berthold Technologies). For the biodistribution analysis, the 4T1 tumor bearing mice were i.v. injected with the same dose of ^{131}I-PDA-PEG-SAN-MET. After 24 hr, the mice were sacrificed and the major organs including heart, liver, spleen, lung, kidney, intestine, skin, stomach, and tumor were collected. Finally we weighed and measured the sample using the gamma counter.

Combination Therapy

All animal experiments were performed with the Guild for the Care and Use of Laboratory Animals according to animal protocols approved by Xidian University. The nude mice were purchased from Nanjing Peng Sheng Biological Technology. To establish the tumor model, 2.5×10^6 of 4T1 cells were collected and resuspended in 50 μL of PBS, which were then subcutaneously injected into the right back of each mouse. After the tumor size grew up to

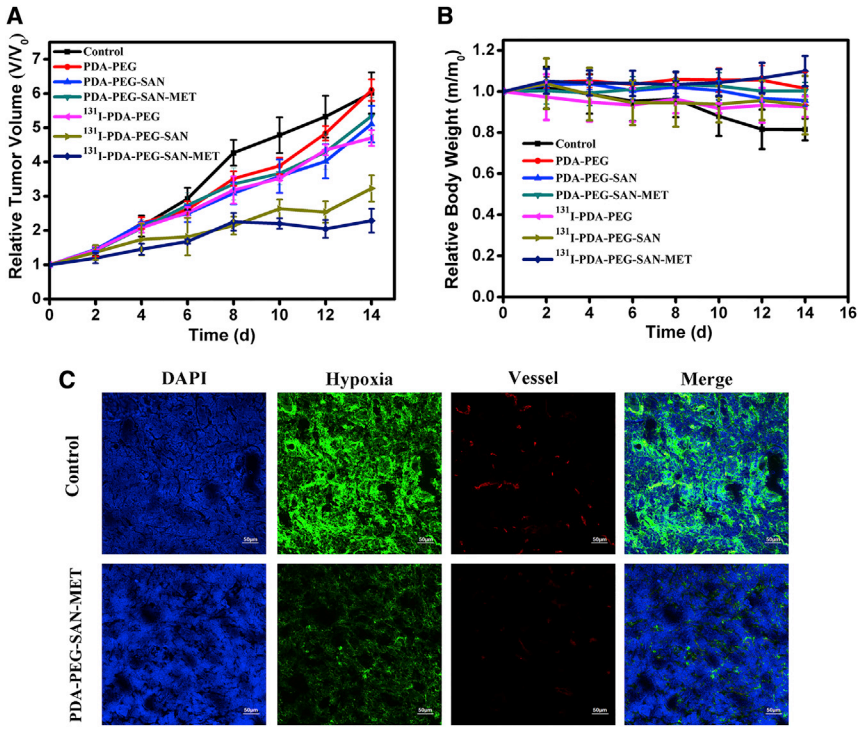

Figure 7. *In Vivo* Combination Radio-Chemotherapy Based on ^{131}I-PDA-PEG-SAN-MET Nanoparticles

(A) Tumor growth curves of 4T1 tumor bearing mice (n = 5) treated with different groups at day 0, 4, 8, and 12. Doses for each injection per mouse: 200 μCi of ^{131}I, 10 mg/kg of PDA-PEG, 4 mg/kg of SAN, 8 mg/kg of MET. The tumor volumes were normalized to their initial sizes, which were set as 1. (B) The weight curves of mice after various treatments during the period of observation lasted for 14 days. (C) Representative immunofluorescence images of tumor slices collected from mice 24 hr post injection of control or ^{131}I-PDA-PEG-SAN-MET. The cell nuclei, blood vessels, and hypoxia areas were stained with DAPI (blue), anti-CD31 antibody (red), and anti-pimonidazole antibody (green), respectively.

about 100 mm^3, the mice were randomly divided into seven groups (five mice per group). These groups were treated with the following: (1) PBS; (2) PDA-PEG (10 mg/kg); (3) PDA-PEG-SAN (4 mg/kg of SAN); (4) PDA-PEG-SAN-MET (4 mg/kg of SAN); (5) ^{131}I-PDA-PEG (200 μCi of ^{131}I); (6) ^{131}I-PDA-PEG-SAN (4 mg/kg of SAN, 200 μCi of ^{131}I); and (7) ^{131}I-PDA-PEG-SAN-MET (4 mg/kg of SAN, 8 mg/kg of MET, 200 μCi of ^{131}I). The aforementioned reagents were i.v. injected in mice every 3 days at day 0, 4, 8, 12. We monitored the tumor volumes by a caliper every other day, and calculated according to the following formula: volume (cm^3) = length (L) × width2 (W^2)/2.

Immunofluorescent Staining

Fresh tumor tissues were collected and imbedded in Tissue-Tek OCT compound (Sakura Finetek), and then cut into 8-μm slices. For hypoxia staining, mice were i.v. injected with pimonidazole (60 mg/kg, Hypoxyprobe-1 plus kit, Hypoxyprobe) 90 min before collecting their tumors. Anti-pimonidazole mouse monoclonal antibody (FITC-Mab1, 200 times dilution, Hypoxyprobe-1 Plus Kit, Hypoxyprobe, Burlington) was used as primary antibody, and Alexa Fluo 488 conjugated goat-anti-mouse antibody was used as the secondary antibody for further staining according to the kit protocol. For blood vessel staining, rat CD31 antibody (Biolegend, 1:200) was used as the primary antibody, while rhodamine conjugated donkey anti-rat antibody (Jackson, 1:200) was used as the secondary antibody. The nuclei were stained with DAPI (Invitrogen, 1:5,000). After staining, all slices were dipped in 4% formaldehyde to fix. Finally the slices were imaged by confocal microscopy.

Statistical Analysis

All data are presented as mean ± SD. The statistical significance of differences between groups are analyzed with Student's t test. $p < 0.05$ was considered statistically significant. Statistical analysis was performed with GraphPad InStat 3 software.

SUPPLEMENTAL INFORMATION

Supplemental Information includes one figure and can be found with this article online at https://doi.org/10.1016/j.ymthe.2018.02.019.

AUTHOR CONTRIBUTIONS

Conceptualization, F.W. and K.Y.; Methodology, F.W. and K.Y.; Investigation, Z.L., B.W., Z.Z., B.W., Q.X., W.M. and J.T.; Writing – Original Draft, Z.L.; Writing – Review and Editing, F.W. and K.Y.; Funding Acquisition, F.W. and K.Y.; Project Administration, F.W. and K.Y.

CONFLICTS OF INTEREST

No potential conflicts of interest were disclosed.

ACKNOWLEDGMENTS

This work was supported by the National Natural Science Foundation of China (81571721, 81772010, 81227901, and 81471716) and the Natural Science Basis Research Plan in Shaanxi Province of China (Program No. 2016JM8016).

REFERENCES

1. Siegel, R.L., Miller, K.D., and Jemal, A. (2017). Cancer Statistics, 2017. CA Cancer J. Clin. *67*, 7–30.

2. Corsini, M.M., Miller, R.C., Haddock, M.G., Donohue, J.H., Farnell, M.B., Nagorney, D.M., Jatoi, A., McWilliams, R.R., Kim, G.P., Bhatia, S., et al. (2008). Adjuvant radiotherapy and chemotherapy for pancreatic carcinoma: the Mayo Clinic experience (1975-2005). J. Clin. Oncol. *26*, 3511–3516.
3. Shibamoto, Y. (2013). Radiation therapy for primary central nervous system lymphoma. Oncol. Rev. *7*, e4.
4. Bekelman, J.E., Sylwestrzak, G., Barron, J., Liu, J., Epstein, A.J., Freedman, G., Malin, J., and Emanuel, E.J. (2014). Uptake and costs of hypofractionated vs conventional whole breast irradiation after breast conserving surgery in the United States, 2008-2013. JAMA *312*, 2542–2550.
5. Buchholz, T.A., Mittendorf, E.A., and Hunt, K.K. (2015). Surgical Considerations After Neoadjuvant Chemotherapy: Breast Conservation Therapy. J. Natl. Cancer Inst. Monogr. *2015*, 11–14.
6. Krishna, R., and Mayer, L.D. (2000). Multidrug resistance (MDR) in cancer. Mechanisms, reversal using modulators of MDR and the role of MDR modulators in influencing the pharmacokinetics of anticancer drugs. Eur. J. Pharm. Sci. *11*, 265–283.
7. Marko-Varga, G., Végvári, A., Rezeli, M., Prikk, K., Ross, P., Dahlbäck, M., Edula, G., Sepper, R., and Fehniger, T.E. (2012). Understanding drug uptake and binding within targeted disease micro-environments in patients: a new tool for translational medicine. Clin. Transl. Med. *1*, 8.
8. Alfarouk, K.O., Stock, C.M., Taylor, S., Walsh, M., Muddathir, A.K., Verduzco, D., Bashir, A.H., Mohammed, O.Y., Elhassan, G.O., Harguindey, S., et al. (2015). Resistance to cancer chemotherapy: failure in drug response from ADME to P-gp. Cancer Cell Int. *15*, 71.
9. Cho, K., Wang, X., Nie, S., Chen, Z.G., and Shin, D.M. (2008). Therapeutic nanoparticles for drug delivery in cancer. Clin. Cancer Res. *14*, 1310–1316.
10. Jabr-Milane, L.S., van Vlerken, L.E., Yadav, S., and Amiji, M.M. (2008). Multi-functional nanocarriers to overcome tumor drug resistance. Cancer Treat. Rev. *34*, 592–602.
11. Lavik, E., and von Recum, H. (2011). The role of nanomaterials in translational medicine. ACS Nano *5*, 3419–3424.
12. Ma, X., Zhao, Y., and Liang, X.J. (2011). Theranostic nanoparticles engineered for clinic and pharmaceutics. Acc. Chem. Res. *44*, 1114–1122.
13. Ryu, J.H., Koo, H., Sun, I.C., Yuk, S.H., Choi, K., Kim, K., and Kwon, I.C. (2012). Tumor-targeting multi-functional nanoparticles for theragnosis: new paradigm for cancer therapy. Adv. Drug Deliv. Rev. *64*, 1447–1458.
14. Ju, K.Y., Lee, Y., Lee, S., Park, S.B., and Lee, J.K. (2011). Bioinspired polymerization of dopamine to generate melanin-like nanoparticles having an excellent free-radical-scavenging property. Biomacromolecules *12*, 625–632.
15. Liu, Q., Wang, N., Caro, J., and Huang, A. (2013). Bio-inspired polydopamine: a versatile and powerful platform for covalent synthesis of molecular sieve membranes. J. Am. Chem. Soc. *135*, 17679–17682.
16. Yan, J., Yang, L., Lin, M.F., Ma, J., Lu, X., and Lee, P.S. (2013). Polydopamine spheres as active templates for convenient synthesis of various nanostructures. Small *9*, 596–603.
17. Huang, S., Liang, N., Hu, Y., Zhou, X., and Abidi, N. (2016). Polydopamine-Assisted Surface Modification for Bone Biosubstitutes. BioMed Res. Int. *2016*, 2389895.
18. Zhong, X., Yang, K., Dong, Z., Yi, X., Wang, Y., Ge, C., et al. (2015). Polydopamine as a Biocompatible Multifunctional Nanocarrier for Combined Radioisotope Therapy and Chemotherapy of Cancer. Adv. Funct. Mater. *25*, 7327–7336.
19. Dong, Z., Gong, H., Gao, M., Zhu, W., Sun, X., Feng, L., Fu, T., Li, Y., and Liu, Z. (2016). Polydopamine Nanoparticles as a Versatile Molecular Loading Platform to Enable Imaging-guided Cancer Combination Therapy. Theranostics *6*, 1031–1042.
20. Tang, W., Liu, B., Wang, S., Liu, T., Fu, C., Ren, X., et al. (2016). Doxorubicin-loaded ionic liquid–polydopamine nanoparticles for combined chemotherapy and microwave thermal therapy of cancer. RSC Advances *6*, 32434–32440.
21. Zhao, H., Chao, Y., Liu, J., Huang, J., Pan, J., Guo, W., Wu, J., Sheng, M., Yang, K., Wang, J., and Liu, Z. (2016). Polydopamine Coated Single-Walled Carbon Nanotubes as a Versatile Platform with Radionuclide Labeling for Multimodal Tumor Imaging and Therapy. Theranostics *6*, 1833–1843.
22. Wang, Y., Zhang, B., Liu, W., Dai, Y., Shi, Y., Zeng, Q., and Wang, F. (2016). Noninvasive bioluminescence imaging of the dynamics of sanguinarine induced apoptosis via activation of reactive oxygen species. Oncotarget *7*, 22355–22367.
23. Song, C.W., Lee, H., Dings, R.P., Williams, B., Powers, J., Santos, T.D., Choi, B.H., and Park, H.J. (2012). Metformin kills and radiosensitizes cancer cells and preferentially kills cancer stem cells. Sci. Rep. *2*, 362.
24. Mowlavi, A.A., Fornasier, M.R., Mirzaei, M., Bregant, P., and de Denaro, M. (2014). Analytical functions for beta and gamma absorbed fractions of iodine-131 in spherical and ellipsoidal volumes. Ann. Nucl. Med. *28*, 824–828.
25. Wang, F., Wang, Z., Hida, N., Kiesewetter, D.O., Ma, Y., Yang, K., Rong, P., Liang, J., Tian, J., Niu, G., and Chen, X. (2014). A cyclic HSV1-TK reporter for real-time PET imaging of apoptosis. Proc. Natl. Acad. Sci. USA *111*, 5165–5170.